Desalination 567 (2023) 116956

Contents lists available at ScienceDirect

Desalination

journal homepage: www.elsevier.com/locate/desal

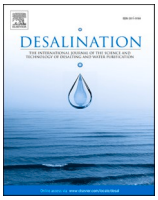

Novel sodium and potassium carbon quantum dots as forward osmosis draw solutes: Synthesis, characterization and performance testing

Afraa H. Kamel [a], Qusay F. Alsalhy [a,*], Salah S. Ibrahim [a], Khalefa A. Faneer [b], S. Abdollatif Hashemifard [c], A. Jangizehi [d], S. Seiffert [d,*], Michael Maskos [d], Alireza Shakeri [e], Christoph Bantz [d]

[a] Membrane Technology Research Unit, Chemical Engineering Department, University of Technology-Iraq, Alsinaa Street 52, 10066 Baghdad, Iraq
[b] Department of Environment Engineering, Higher Institute of Science and Technology, Bent Baya, Wadi AL-Ajal, Libya
[c] Sustainable Membrane Technology Research Group (SMTRG), Water research institute (WRI), Faculty of Petroleum, Gas and Petrochemical Engineering (FPGPE), Persian Gulf University, P.O. Box 75169-13798, Bushehr, Iran
[d] Department of Chemistry, Johannes Gutenberg University Mainz, Duesbergweg 10–14, D-55128 Mainz, Germany
[e] School of Chemistry, College of Science, University of Tehran, P.O. Box 14155-6619, Tehran 141556455, Iran

HIGHLIGHTS

- Novel draw solutes were prepared and evaluated for enhancing FO performance.
- K-CQDs and Na-CQDs draw solutes revealed a high water flux, and very low reverse and specific solute flux
- Stability test revealed that the water flux of K-CQDs was a slight decrease of 2 % after three-cycle of FO operations.
- High feasibility of using K-CQDs and Na-CQDs in the FO process and their applicability for seawater desalination

ARTICLE INFO

Keywords:
Forward osmosis
Draw solute
Desalination
Membranes
Carbon quantum dots

ABSTRACT

Novel draw solutes based on potassium- and modified sodium-functionalized carbon quantum dots (K-CQDs and Na-CQDs) were prepared for seawater desalination. The characteristics of draw solutes were determined using Fourier Transform infrared spectroscopy (FTIR), field emission scanning electron microscopy (FE-SEM), energy-dispersive X-ray (EDX) spectroscopy, and thermal gravimetric analysis (TGA). The results of the FO system with K-CQDs and deionized water (DI) as a feed revealed a high water flux of 10.94–13.924 L/m^2.h (LMH), very low reverse solute flux of 0.0161–0.0253 g/m^2.h (gMH), and specific reverse solute flux of 0.0015–0.0018 at a concentration of 0.3–0.5 g/mL. The water flux of K-CQDs at a concentration of (0.3–0.5) g/mL for seawater and 0.5 g/mL for Real Persian Gulf (RPG) water (Arabian Gulf) was (3.779–5.371) LMH and 6.1662 LMH, respectively. For Na-CQDs with DI, the obtained water flux, reverse solute flux, and specific reverse solute flux were 10.3433–11.935 LMH, 0.0414–0.0621 gMH of 0.004–0.0052, respectively at a concentration of 0.3–0.5 g/mL at 29 °C. The fluxes of synthetic seawater and RPG with K-CQDs and Na-CQDs were 5.37 and 6.16 LMH and 2.78 and 3.78 LMH, respectively, at CQDs concentration of 0.5 g/mL. The stability test showed that there was only a slight decrease in the flux of 2 % after three-cycle of FO operations with K-CQDs.

1. Introduction

Water is the principal commodity for living ecosystems. Rapid population growth and industrialization have manifested a huge challenge with available freshwater resources. The trade-offs between this growth and water resources have given rise to a high contest and necessitated urgent actions to tackle this inevitable crisis [1–3]. Compared to traditional thermal desalination, reverse osmosis (RO) process implementation has demonstrated a well-distinguished economic and environmental advantage in the seawater desalination industry. The recent advances witnessed in membrane-based separation technology have resulted in leapfrogging opportunities in the field of desalination

* Corresponding authors.
E-mail addresses: qusay.f.abdulhameed@uotechnology.edu.iq (Q.F. Alsalhy), sebastian.seiffert@uni-mainz.de (S. Seiffert).

https://doi.org/10.1016/j.desal.2023.116956
Received 25 May 2023; Received in revised form 1 August 2023; Accepted 4 September 2023
Available online 6 September 2023

and water treatment. The versatility of the membrane-based separation processes and their tolerance for diverse applications made them an undisputedly futuristic separation choice [1,2,4]. In this context, one of the recent exceptional membrane separation processes is forward osmosis (FO). FO is a relatively innovative paradigm within the current membrane processes. Particularly, the process consumes slight energy compared to RO membrane while maintaining product quality. To perform the separation, FO harnesses the natural osmotic pressure as a driving force induced by the concentration gradient between a feed and draws solution. This is opposed to the working principles of common membrane processes, such as RO, where hydraulic pressure is needed [5]. However, the application of the FO technology for desalination is not as smooth as it may be perceived and faces several challenges such as finding suitable DS.

The nature and characteristics of DS are pivotal to the FO process as it acts as a pump in the RO process [6]. Features of DS have a direct link to the FO membrane performance, and thus choosing the right DS is crucial [7]. Choosing DS and the way that could be recovered determines whether the FO application is successful or not. Particularly, this could not only enhance the process efficiency but also, translated into a radical reduction in process application cost. Yet, despite the vast number of novel DS been developed and evaluated for FO applications, none of them has been commercialized [8]. Typical DS for successful FO application should possess a high flux, diminished reverse salt flux (RSF), and is highly recoverable [9]. Other considerations should be also taken into account before introducing any FO system into real-world industries, including DS nontoxicity, cost feasibility, and commercial availability [8]. DS has been commonly categorized into several sections. Inorganic compounds have taken the biggest share due to their potential to produce a high water flux and ease of recovery via pressure-driven membrane processes [10]. The conventional inorganic salts such as NaCl and $MgCl_2$ produced high osmotic pressure along with high water flux. However, the high reverse solute leakage and the high cost of draw solute recovery raised the total operational costs [11]. Likewise, thermolytic compounds, such as NH_4HCO_3, TMA-CO_2 and SO_2 have also inspired the scientific community as a novel DS for FO desalination. However, their practical application is restricted due to solubility in water, corrosivity, reactivity, volatility and potential health issues [12–15]. Organic compounds (e.g., glucose, sucrose, …etc.) have been also reported in the literature as DS for wastewater treatment, potable water and food production applications [16–18]. This type of DS is characterized by large molecular size and is expected to endow more feasible performance than inorganic salts, especially, in reducing the RSF. Other forms of DS have also been reported in recent literature. Polyelectrolyte-based DS has been proposed for its high hygroscopic potential and large molecular size [19].

There are several papers that have published in recent years regarding development of new/modified draw agents for forward osmosis process [20–24]. Also, recent studies have reported stimuli-responsive polymeric hydrogels and functionalized magnetic nanoparticles (MNP) with hydrophilic and ionic strength groups as exceptional DS [25–27]. The hydrogels contain hydrophilic polymer networks and show high water absorption. As a draw solutes, they were found to be energy efficient and environmentally friendly, but they have disadvantages such as the poor liquid water recovery rate and unsuitability for practical application [26]. Despite the recent advances witnessed in FO draw solutes synthesis, present DS still poses many drawbacks, such as low osmotic pressure, high reverse solute flux, and complex and energy-intensive regeneration processes.

With the flourishing research interest paid to nanotechnology and its applications, nanotechnology-based DS for FO application has come along the way as a compromised DS with promising results. Functionalized magnetic nanoparticles (MNPs) exploiting highly ionic strength and water-soluble groups have acquired exceptional attention as DS for FO applications. Unsurprisingly, this was due to the ease of recovery from the water using an external magnet along with the capability of these NPs to generate high osmotic pressure [28]. The first inception of MNPs as DS was conceived by Warne et al. [27] in 2008. Following that, a number of studies were published on coating versatile functional groups on the surface of the MNPs. For brackish water desalination by FO membrane, Bai et al. (2011) devised novel dextran-coated Fe_3O_4 magnetic nanoparticles. Results manifested that merging the excellent solubility of dextran and NPs magnetism could endow stringent criteria for DS. Utilizing such DS features could be an ideal choice for energy-saving and eco-friendly desalination processes [29]. In another work, thermosensitive super MNPs were synthesized via a facile thermal decomposition route and employed as smart DS for water reuse applications. Authors reported that NPs could be successfully recycled without compromising performance efficiency [30]. Carbon-based quantum dots have emerged as a new class of carbon nanomaterials are one of these interesting nanomaterials. CQDs come with diameters below 10 nm and an abundance of functional groups, such as amino, hydroxyl, carboxyl, carbonyl, and other oxygenous groups [31]. Also, they are known as carbon nano lights that received a fair amount of attention due to their high solubility, low toxicity, great water dispensability, ease of synthesis, functionalization and intense luminosity [32,33]. To the best of authors knowledge, there is only one publication addressed CQDs as a DS for the FO application has been reported [34]. In that work, a novel type of biocompatible Na+-functionalized carbon quantum dots (Na-CQDs) was synthesized by Guo et al., (2014) with ultra-small size and rich ionic species. The prepared Na-CQDs were harnessed in the PRO mode [active layer facing DS (AL-DS)] instead of the FO mode. According to their results, Na-CQDs aqueous dispersion displayed high osmotic pressure which reflected on the water flux while maintaining a slight reverse solute permeation. Another work curried out by Doshi and Mungray [35] to fabricate the CQDs from Tulsi (Ocimumtenuiflorum) and use it as a draw agent in forward osmosis desalination. Based on aforementioned, optimal DS selection is still the main obstacle facing the FO process spreading in industrial applications, and more efforts should be placed in that direction. Moreover, there are also several publications on the application of CQDs most of them on fabrication of FO membranes [36].

In our view, the novelty of this work can be seen in three aspects. First, the synthesis procedure of CQDs has been modified. Second, the surface functional groups have been neutralized with two cations and the performance has been compared. Third, the forward osmosis desalination has been performed on Persian Gulf water. The main advantages of suggested draw agents are their simple method of fabrication, their high performance of desalination of seawater and a relative efficient of their regeneration.

This work presents a novel route for preparing two DS for seawater desalination, by FO system based on potassium- and modified sodium-functionalized carbon quantum dots. The characteristics of DS were fully determined via a set of characterization tools. This includes FTIR, FE-SEM, EDX, TGA, zeta potential, and AFM. Following that, a comprehensive investigation was conducted in FO mode to evaluate both DS in terms of water flux, solute permeability and reverse solute flux. The stability and recyclability of a draw solute in real applications were also investigated.

2. Experimental work

2.1. Materials

Cellulose Triacetate (CTA) flat sheet membrane was supplied by Fluid Technology Solutions (FTS H_2O, Albany, OR, USA) and mounted in the FO cell. Citric acid $1H_2O$ (>99.5 %), Sodium Hydroxide (>98 %), and Sodium Chloride (>99.5 %) were purchased from Romil, UK. Potassium Carbonate (99.9 %) was supplied by SDFCL, India. Potassium Chloride (>99.5 %) was purchased from Chem-Lab, Belgium. Magnesium Chloride Hexahydrate (99.0 %) was obtained from CDH, India. Deionized (DI) water with high purity was used for all experiments.

2.2. Synthesis of draw agents

A simple, rapid and eco-friendly route was employed to prepare both DS. For the synthesizing Na-CQDs and K-CQDs, a 100 g citric acid monohydrate was initially ground into fine powders and then heated in air at 180 °C for 90 min in a glass beaker covered with a glass slide. The selection of 180 °C to heat the citric acid monohydrate was based on the obtained thermal gravimetric analysis (TGA) results, as shown in Fig. S1. Following this stage, a yellowish powder comprising CQDs was formed. The CQDs were then homogenously dispersed in water for 15–20 min, then neutralized (pH = 7) with 5.0 M NaOH solution under continuous stirring to obtain Na-CQDs. Similarly, to synthesise K-CQDs, a 5.0 M of potassium carbonate was added to CQDs precursor gradually under continuous stirring and neutralization to pH = 7. Subsequently, the produced solutions (Na-CQDs and K-CQDs) (feed solution) were dialyzed until the conductivity of the DI water was constant. The dialysis test was performed with a lab-scale setup (Fig. 1) using a commercial dialysis membrane (smart flux PUREMA dialyzer LFP-180, cutoff molecular weight 500 Da, Medica, Italy) and the dialysate solution was DI water.

Later, Na-CQD and K-CQDs solutions were dried at 80 °C. The drying process took place in two stages. First, a preliminary drying stage by the rotary evaporator where the water ratio in the prepared DS after the dialysis process was reduced depending on the vacuum pressure. In the final drying stage (80 °C) a powder was obtained and kept in a glass Petri dish ready for further use.

2.3. Preparation of draw solution and feed solution

K-CQDs and Na-CQDs draw solutions with a concentration varying from 0.3 to 0.5 g/mL were prepared along with NaCl solution with a concentration of 80 g/L. Three different feed solutions were utilized for the FO system evaluation such as deionized water, synthetic seawater water (3.5 wt% NaCl) and real Persian Gulf water. The Persian Gulf water sample was filtered using a 220 nm PTFE filter membrane before the FO testing. The specifications of Persian Gulf water following the filtration was summarized in Table S1. The composition and ions in the Persian Gulf water sample after evaporation were analyzed via energy-dispersive X-ray spectroscopy (EDS) as depicted in Fig. S2.

2.4. Characterization of draw solutes and membranes

A set of experimental tools have been employed for characterizing the membranes and draw solutions. This includes FTIR Spectroscopy (FTIR Raffinity-1 Shimhdzo ATR, Japan), EDX Spectroscopy (Bruker, Germany), Contact Angle (Si-plasma Cam 110, Taiwan), AFM (SPM AA300 Angstrom Advanced Inc., USA), Osmometer (KNAUER, K-7400 Semimicro Osmometer, Germany), TGA (Sdt Q600 V20 9 Build 20, New Castle, DE, USA), and Zeta Potential (Malvern, United Kingdom). In AFM measurements, the particle size and particle size distribution were estimated by using IMAGER 4.31 software, a statistical particle size distribution was established for the surfaces of all samples.

2.5. Experimental setup of FO system

A custom-made apparatus was designed with a rectangular acrylic FO cell module as shown in Fig. S3. The cell consisted of four vents, input, and output for both feed and draw solutions. The module has an effective area of 33.516 cm^2 with feed and draw solutions flowing in the co-current direction. The lab-scale FO system was equipped with a flat sheet CTA-FO membrane and the system was working in FO mode, where the active layer faces the feed solution (AL-FS) and the support

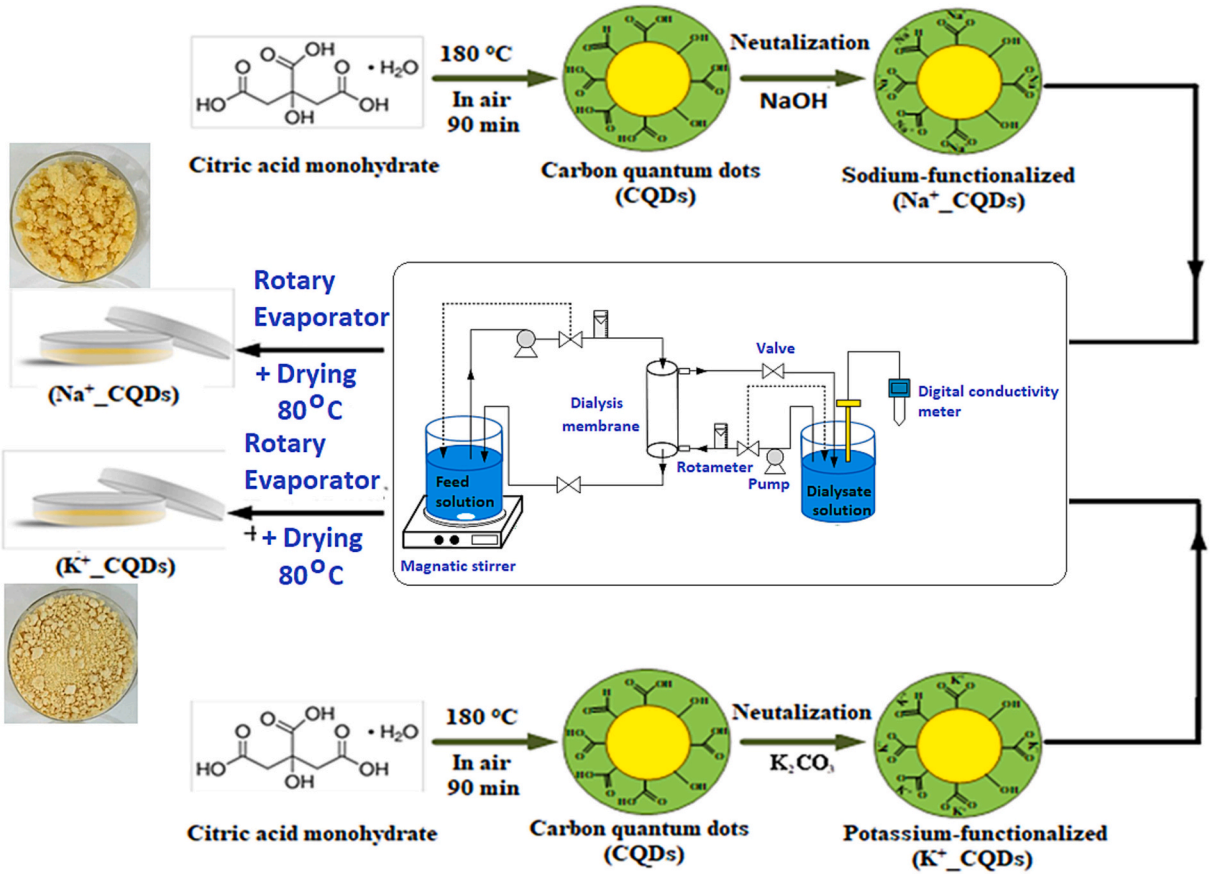

Fig. 1. The schematic diagram of Na-QCDs and K-QCDs synthesis.

layer of the membrane faces the draw solution (SL-DS). Feed and draw solutions were co-currently flowing through the channels of the cell during the operation. Using a chiller and water bath, the feed and draw solutions were maintained at 29 ± 1 °C. The experimental time was set to 3 h. The reduction in the volume of the feed solution (FS) was measured every half an hour and the mean value of the water flux was reported. Also, the concentration of FS was measured using a conductivity meter. The operating conditions of the FO process are given in Table S2. All specifications and characterization of CTA membrane are presented in Table S3.

2.6. FO performance evaluation

To measure the water permeability value (coefficient A) of the CTA membrane, deionized water was pumped into the feed side of the flat sheet module at an inlet flow rate of 0.5 L/min and 29 °C. Each of these experiments was performed with a hydraulic pressure of 0.5–2 bar. The permeated solution from the draw side was collected in a graduated cylinder. The water flux (J_w^{RO}) at each applied pressure was obtained by using Eq. (1) [37]:

$$J_w^{RO} = \frac{V}{A_m.t} \quad (1)$$

where V represents the volume of collected water at time *t*, A_m represents the membrane's effective area. The main water flux J_w^{RO} formula that describes the RO process is:

$$J_w^{RO} = A(\Delta P - \Delta\pi) \quad (2)$$

where A is the water permeability, ΔP is the applied pressure across the membrane; $\Delta\pi$ is the difference in osmotic pressures across the membrane. Due to utilizing deionized water as a feed, $\Delta\pi$ is zero. Water flux J_w^{RO} was determined for each applied pressure ΔP experimentally, and the slope of the water flux versus applied pressure curve represents the pure water permeability coefficient A.

The permeate water flux (J_w, Lm^{-2} h^{-1}) was calculated from the volume change of feed stream using the following equation:

$$J_{w=}\frac{\Delta V}{A.\Delta t} \quad (3)$$

where $\triangle V$ is the change in the volume of feed solution over time ($\triangle t$), and A is the effective surface area of the used FO membrane.

The solute permeability coefficient (*B*) was measured for two types of DS (K-CQDs and Na-CQDs) under RO mode at 29 °C. The RO experiments were performed with 50 ppm for each DS. DI water was used as a solvent to prepare the two types of DS. The draw solution was pumped into the feed side of the flat sheet module under 2 bar hydraulic pressure with a 0.5 L/min flow rate. The salt rejection (R) for DS of the CTA membrane was obtained by measuring the concentration of the bulk feed (C_f) and permeate (C_P) solutions using Eq. (4) [32]:

$$R = 1 - \frac{C_P}{C_f} \quad (4)$$

A digital conductivity meter was used to measure the two types of DS concentration in the permeate solution C_p. The salt permeability coefficient (*B*) was then calculated as follows:

$$B = \frac{A(\Delta P - \Delta\pi)(1 - R)}{R} \quad (5)$$

It is important to mention here that water permeability (A), salt rejection (R), and salt permeability (B) are intrinsic permeability properties (i.e. selective layer properties) of FO membranes.

For Reverse Solute Flux, J_s (gMH) and Specific Reverse Solute Flux (J_s/J_w) measurements (The specific reverse solute flux is defined as the ratio between reverse solute flux (J_s) and water flux (J_w)), DI water was initially employed as the feed solution, then, reverse solute flux was calculated by measuring the change of solute content in the feed stream by the conductivity data utilizing the following equation [38]:

$$J_{s=}\frac{V_tC_t - V_0C_0}{A.\Delta t} \quad (6)$$

where V_o and V_t represented the initial and final volumes of the feed stream, C_o and C_t represented the initial and final solute concentrations of the feed stream.

For the regeneration of diluted K-CQDs draw solution at 0.5 g/mL of K-CQDs and DI water as feed solution, direct contact membrane distillation (DCMD) system shown in Fig. S3 with PTFE flat sheet membrane Manufactured by sterlitech, USA with characteristic of (Pore size: 0.2 μm, Support material: Laminated, PP neting and Water entry pressure: >2.5 bar (37 psi)) was used. The diluted draw solution (feed side in MD system) was circulated through the flat sheet MD module by diaphram pump after being heated up to 50 °C and 60 °C by using a water bath, while DI water, as the permeate solution, was counter currently circulated through the MD module by a diaphram pump after being cold to 20 °C by the chiller. The feed and permeate flow rates were kept constant at 500 ml/min and 300 ml/min, respectively. The difference between the feed solution and permeate side are $\triangle T$ = (30–40) °C. The time of the experiment was 3 h; every half an hour, the reducing in the volume of the feed solution (FS) was measured. Also, the concentration of permeate side was measured using a conductivity meter. The MD system was cleaned using deionized water twice at the end of each experiment for 20 min, to remove particles that accumulated on the surface of the PTFE membrane. The conductivity of K-CQDs draw solution at 0.5 g/mL of K-CQDs was measured at 20 °C temperature.

3. Results and discussion

3.1. Characterization of draw solution

3.1.1. FTIR and EDX

FTIR spectroscopy was employed to affirm the functionalization of CQDs nanoparticles with Na and K. This could be carried out by defining the functional group's variation on the CQDs before and after the grafting. Fig. S4 depicts the FTIR absorption spectra of monohydrate citric acid (CAM), CQDs, Na-CQDs, and K-CQDs. citric acid monohydrate FTIR absorption spectra were recorded in the range of 1900–1600 cm^{-1} (Fig. S4a). The infrared spectrum of the molecule, in this wavenumber range is characterized by an overlapped triplet of sharp and intense absorption bands at 1755, 1720, and 1685 cm^{-1} assigned to the stretching mode of C═O in monohydrate citric acid. Referring to TGA analyses during the formation process of Na-CQDs and K-CQDs from citric acid, citric acid molecules had undergone incomplete carbonization by losing some –OH groups. Indeed, resulting in CQDs with carboxyl groups at moderate heat treatment (at 180 °C for 90 min) as seen by the broad band around 2900 cm^{-1} (Fig. S4b).

Fig. S4c and d displayed the development of Na-CQDs and K-CQDs, respectively. FT-IR spectra of CQDs, K-CQDs, and Na-CQDs show —COO and —C—O groups inherited from citric acid molecules [39]. In addition, the CQDs exhibit characteristic stretching vibration of C—H at 2950 and below 1350 cm, indicating that the CQDs contain incompletely carbonized citric acid. That is in agreement with [34,40]. Due to the existence of abundant carboxyl groups, CQDs have a relatively acidic nature. After adding NaOH, or K_2CO_3 the acidic CQDs were neutralized by converting —COOH groups into —COONa, or COOK producing Na-CQDs and K-CQDs.

EDX spectra for citric acid and CQDs, Na-CQDs, and K-CQDs are shown in Fig. 2. as could be seen, the O/C weight ratio of citric acid was 1.08 (51.93/48.07), while CQDs exhibited a lower O/C weight ratio of 1.045. This suggests that a small portion of oxygen groups was lost during the heating process. It is well known that citric acid molecules

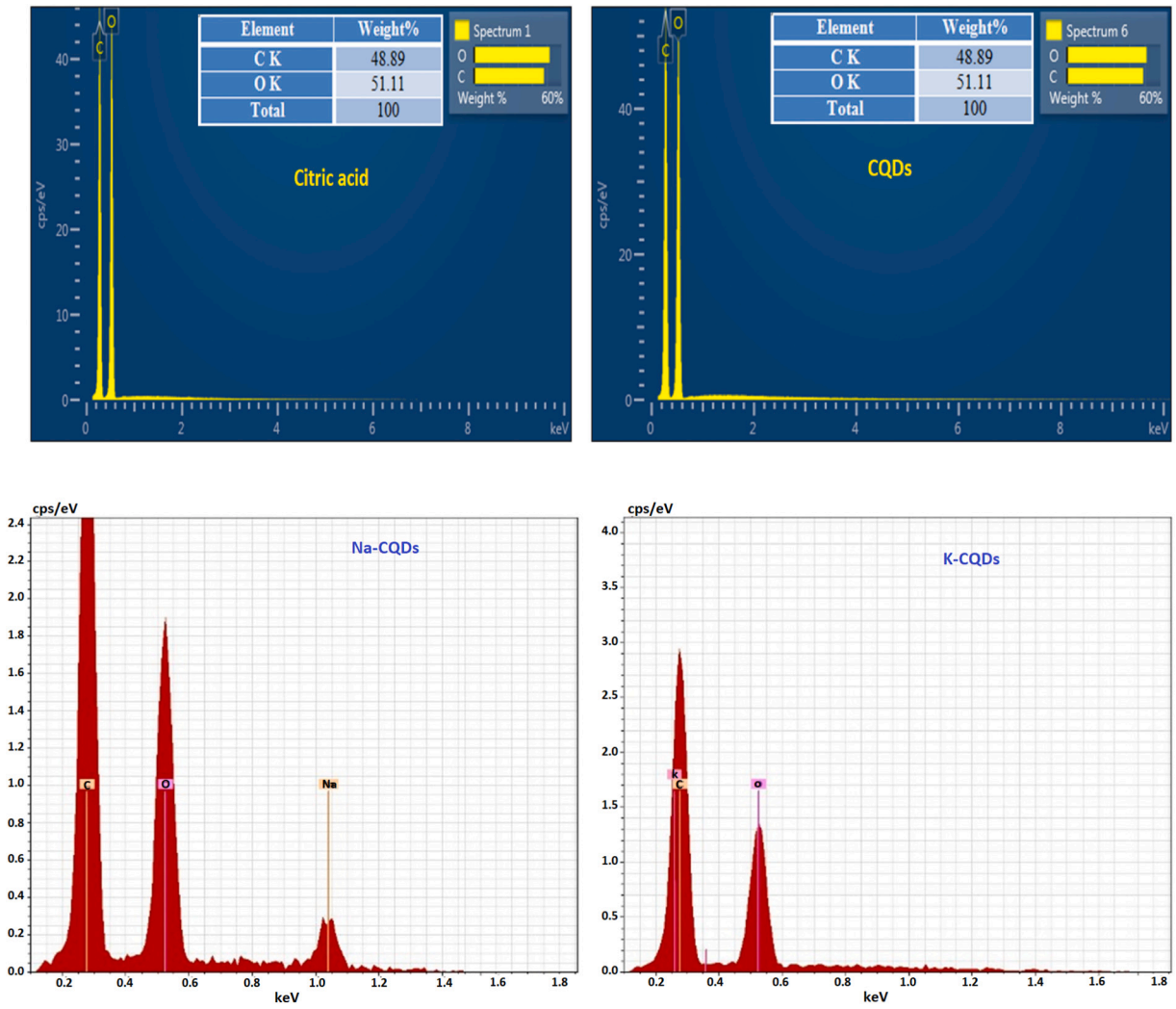

Fig. 2. EDX spectra of citric acid, CQDs, Na-CQDs, and K-CQDs.

contain abundant —OH groups, which can cause polymerization (carbonization) during the heat treatment at 180 °C. This is similar to that of glucose that forms carbonaceous spheres under hydrothermal treatment. These results agreed with that reported in preceding studies [34,41,42].

The presence of C, O, Na, and K in CAM, CQDs, Na^+–CQDs, and K^+-CQDs, respectively, were quantitatively confirmed by EDX, (Fig. 2). The Na and K content in Na-CQD and K-CQD was 14.53 % and 13.98 %, respectively. Besides, the CQDs and functionalized CQDs have high oxygen content, indicating that high quantity oxygen-containing groups existed in these CQDs. Both the ultra-fine size of CQDs and the existence of sodium, potassium and oxygen-containing groups contribute to the excellent hydrophilicity of CQDs. This bestowed good dispersion of CQDs in aqueous solutions.

3.1.2. Stability with other salts

The effect of $MgCl_2.6H_2O$, NaCl, and KCl on draw solutions was checked by measuring the osmolality of each type. Initially, 0.1 wt% solutions from each salt were prepared using DI water as a solvent. Following that step is mixing with each sample of K-CQDs and Na-CQDs and then measuring their osmolality with an osmometer device. Later, waiting for two days and measuring the osmolality of the same sample. It was found that the difference between the two readings was 0.88 %, with no change, and 0.62 % for K-CQDs at KCl, $MgCl_2.6H_2O$, and NaCl, respectively. Meanwhile, recorded 0.89 %, 1.14 %, and 1.25 % for Na-CQDs at KCl, $MgCl_2.6H_2O$, and NaCl, respectively. The stability tests showed that the K-CQDs showcased slightly better results than Na-CQDs. This was attributed to the structure of the synthesis material.

3.1.3. Atomic force microscopy (AFM)

AFM is a well-recognized and a potent tool to scan the surface topography of materials and provide necessary data about surface roughness parameters and approximate particle size distribution. Fig. S5A and B depicted the three-dimensional (3D) AFM images and particle size distributions of K-CQDs and Na-CQDs, respectively. The average roughness (Ra) and root mean square (Rq) were 1.14 nm and 1.67 nm for K-CQDs while they were 1.3 nm and 1.77 nm for Na-CQDs. In comparison to Na-CQDs, K-CQDs manifested slightly lower roughness parameters.

The average particle size of K-CQDs and Na-CQDs were almost convergent at 10.66 nm and 10.98 nm, respectively. These obtained values were very close to 10 nm, which is consistent with the reported particle size range of CQDs (~10 nm) [31]. According to Fig. S5, about 77 % of K-CQDs total particles were <11 nm, 91 % were <12 nm, and 97 % are <15 nm. For Na-CQDs, 63 % of all cumulated particles were <11 nm, 85 % <12 nm, and 96 % <15 nm.

3.1.4. Zeta potential

The zeta potential is an explicit measurement indicating the stability level of particles in a dispersion [43]. The magnitude of the zeta

potential indicates the degree of electrostatic repulsion between adjacent charged particles that carries a similar charge. For molecules and particles that are small enough, a high zeta potential indicates a good stability, i.e., the dispersion resists aggregation. When the potential is small, attractive forces may exceed repulsive forces and the dispersion may break and flocculate [44].

The zeta potential of K-CQDs and Na-CQDs are shown in Fig. 3A. The surface charges of K-CQDs measured by zeta potential analysis manifested a highly positively value (64.35 mV), compared to 28.89 mV for the Na-CQDs. This is beneficial to prevent the deposition of both CQDs on the surface of the CTA membrane since both CTA membrane and CQDs are positively charged. Because of the similarity of charges between the CTA membrane and K-CQDs and Na-CQDs, repulsion occurs and thus reduces the deposition of solute that occurs on the surface of the membrane. This ultimately enhances the water flux and reduces the reverse solute flux. Based on that, it is anticipated that better performance for K-CQDS than Na-CQDs could be achieved due to the higher positively zeta potential value observed.

3.1.5. Thermal gravimetric analysis

The thermal stability of Na-CQDs and K-CQDs was evaluated via TGA as shown in Fig. 3B. The entire temperature range was ramped from 25 to 800 °C. As could be seen, TGA analysis of the K-CQDs indicated that the sample was stable up to 200 °C. The degradation curve consisted of three parts: The first drop initiated from 31.62 °C to 273.4 °C with a slight weight loss (7.295 %) caused by losing the moisture content. The second region started from 343.7 °C to 462.9 °C whereas the weight loss recorded 11.94 % due to the loss of CO_2 and OH functional group. The third decline region started from 462.9 °C to 800 °C and the weight loss was 13.24 % due to the loss of CO. Herein, the total weight loss within the entire temperature range (25 °C to 800 °C) was 32.48 %. This indicated that K-CQDs were thermally stable and this agreed with the thermal characteristics of CQDs reported in preceding literature [45]. However, the Na-CQDs displayed less thermal stability behaviour compared with the of K-CQDs. The degradation curve of solid Na-CQDs consists of four regions: The first decline started from 27.2 °C to 216.5 °C where 13.29 % weight loss was observed due to the loss of the water content. The second part started from 223.4 °C to 373.6 °C and the sharp weight loss recorded 13.02 % due to the water loss, while the third part started from 373.6 °C to 531.01 °C and the weight loss was 8.521 % due to the loss of CO. The final decline started from 531.01 °C to 800 °C with a weight loss of 13.26 %. The total weight loss with increasing the temperature from 25 °C to 800 °C was 48.08 %.

The thermal stability of K-CQDs is better than Na-CQDs. The decomposition of K-CQDs and Na-CQDs only started at 200 °C and 175 °C, respectively. This is much higher than the typical thermal processes for water treatment such as membrane distillation [46].

3.1.6. Density and viscosity

The low viscosity and high osmotic pressure are highly desirable

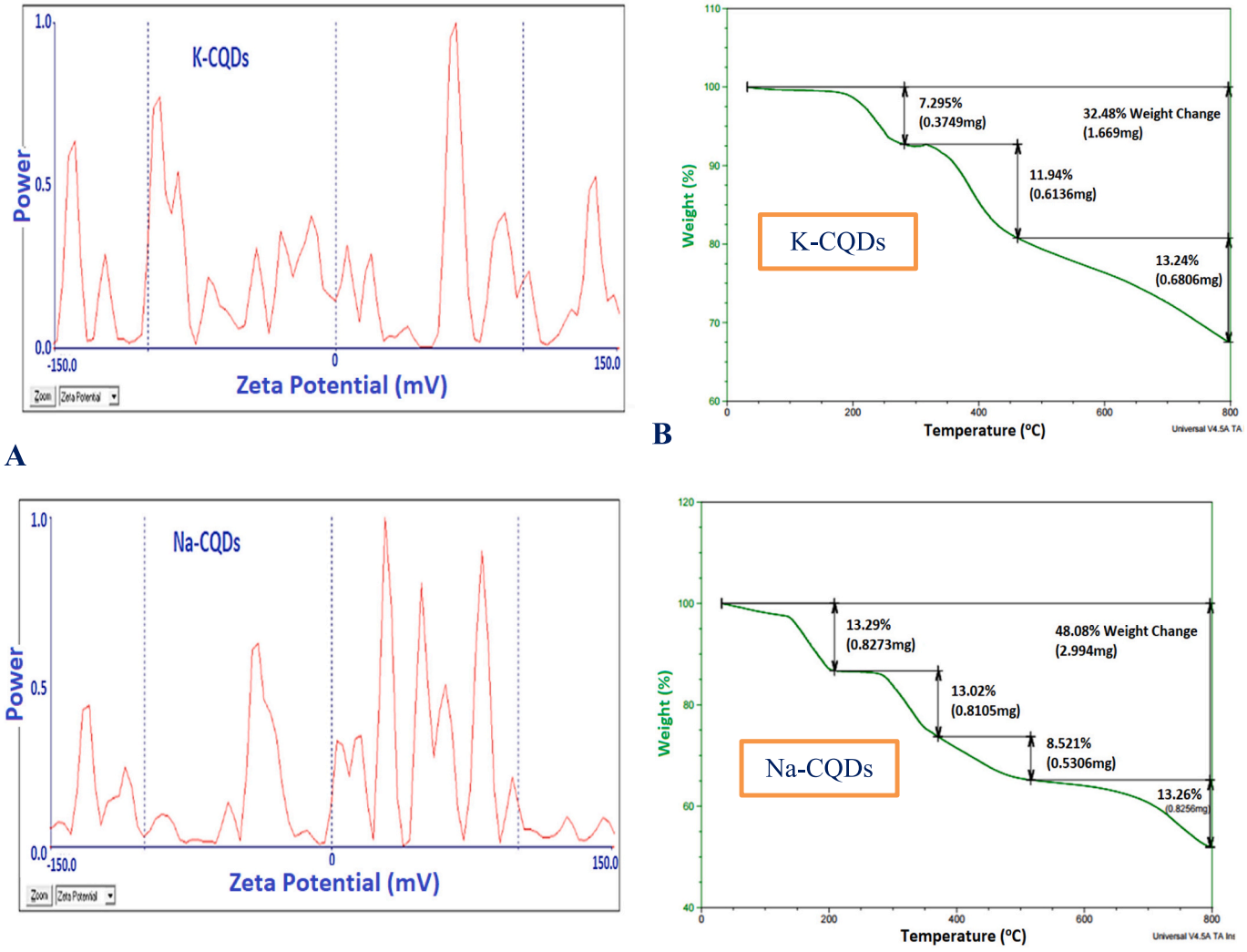

Fig. 3. (A) Zeta potential of K-CQDs and Na-CQDs, (B) TGA of K-CQDs and Na-CQDs.

traits of an ideal DS [47]. With the variation of concentration from 0.3 to 0.5 g/mL, the density of the K-CQDs and Na-CQDs solutions increased from 1.1478 to 1.2257 g/cm^3 and from 1.1421 to 1.2188 g/cm^3, respectively, (Table S3). Most probably, this was induced by the more efficient packing of the K-CQDs and Na-CQDs compounds. Worth mentioning, these values were lower than other complexes reported in the literature [48]. Similarly, the relative viscosity (ηr, calculated applying Eq. (8) [43–45]) of K-CQDs and Na-CQDs displayed an increase (1.4635–2.2329) and (2.1414–3.7949) upon increasing the concentration for boyh CQDs, respectively. Despite the same CQDs amount and an identical weight percent of Na and K elements in Na-CQDs and K-CQDs having been harnessed, the viscosity of Na-CQDs was higher than K-CQDs. The K-CQDs and Na-CQDs exhibited a relative viscosity higher than the NaCl solution (1–1.1) M in the concentration range of 0.5–1.5 M [46]. The physical propertiessuch as density, kinematic viscosity, dynamic viscosity and relative viscosity of the Na-CQDs and K-CQDs draw solutions are presented in Table S4

$$\eta_r = \frac{\eta}{\eta_\circ} \tag{8}$$

where: η and η_o are the viscosities of each DS solution (K-CQDs or Na-CQDs) and the DI water, respectively.

As shown in Table S4, the relative viscosity (η_r) of K-CQDs and Na-CQDs are increasing with increasing of the concentration at 29 °C. For K-CQDs and Na-CQDs at concentration ranged from (0.3–0.5) g/mL the relative viscosity are (1.4635–2.2329) and (2.1414–3.7949) respectively. Although the same CQDs and the same weight percent of Na and K element in Na-CQDs and K-CQDs respectively, the viscosity of Na-CQDs is larger than K-CQDs as shown in Table S4. The K-CQDs are much lower than the polyelectrolyte, which has a relative viscosity of 40 at 0.5 M [46] and lower than the hydroacid complex (Na_5CAFe) that has a relative viscosity range in the range of 1.5–5 at 0.5–1.5 M [44]. Also, lower than dendrimer 2.5G PAMAM-COONa aqueous solutions (33.3 wt %) which has a relative viscosity 9.16, lower than thermos-responsive copolymer poly(sodium styrene-4-sulfonate-*co*-n-isopropylacrylamide) (PSSS-PNIPAM) solution 15SN (10–33.3 wt%) that has a relative viscosity of 5–70 [43], lower than polyelectrolyte poly(isobutylene-*alt*-maleic anhydride) (IBMA) using NaOH [IBMA-Na] solution with a relative viscosity of 12–128 at concentration of 0.05–0.4 g/mL [45] and lower than [(0.1–1)M $MgCl_2$ + 0.05 M $Al_2(SO_4)_3$] solution has dynamic viscosity of 1.8–2.35 cP [47]. While the relative viscosity of Na-CQDs was very lower than the polyelectrolyte that has a relative viscosity of 40 at 0.5 M [46]. Also, lower than dendrimer 2.5G PAMAM-COONa aqueous solutions (33.3 wt%) that has a relative viscosity of 9.16 [43], lower than the thermoresponsive copolymer poly (sodium styrene-4-sulfonate-*co*-n-isopropylacrylamide) (PSSS-PNIPAM) solution 15SN (10–33.3 wt%) with a relative viscosity of 5–70 [43] and lower than polyelectrolyte poly(isobutylene-alt-maleic anhydride) (IBMA) using NaOH [IBMA-Na] solution has a relative viscosity (12–128) at a concentration of (0.05–0.4)g/mL [45]. The K-CQDs and Na-CQDs have a relative viscosity higher than the NaCl solution that has a value of 1–1.1 in the concentration range of 0.5–1.5 M [44]. The K-CQDs more suitable for the FO–MD system compared with other because a high viscosity of the draw solution not only leads to high energy consumption for fluid pumping but also results in severe internal concentration polarization [43].

3.1.7. Solubility

Based on solubility measurements, the K-CQDs were more soluble in water than Na-CQDs while both were very soluble compared to other DS. At a temperature of 29 °C, the solubility of K-CQDs in water was 203 g K-CQDs/100 g H_2O while the solubility of Na-CQDs was about 87 g Na-CQDs/100 g H_2O. This difference could be stemmed from the various functional groups attached to the surface after the synthesis, such as hydroxyl, carboxyl and carbonyl. It is worth noting that both K-CQDs and Na-CQDs exhibited excellent quantitatively proved in water even at a high concentration (0.5 g/mL) along with high solubility and homogenous aqueous solutions.

3.1.8. The osmotic pressure

The correlation between the osmolality and concentration for (K-CQDs), (Na-CQDs), and (NaCl) is depicted in Fig. 4. This osmotic pressure (bar) obtained from an osmometer device was calculated based on the equation below:

$$\pi, \text{bar} = \text{iMRT} = (\text{Osmolality, mosmol}) \times 0.001 \times 1.01325 \times 0.082 \times (\text{T, K}) \tag{9}$$

where, i is Van't Hoff factor, M is Molar concentration of the solute in the solution, R is Universal gas constant, and T is the temperature in K.

The maximum measured concentration was 0.1 g/mL for K-CQDs and Na-CQDs and 50 g/L for NaCl. From the obtained relation, the osmotic pressure for K-CQDs and Na-CQDs could be determined. From Fig. 4 the osmolality of K-CQDs and Na-CQDs at (0.3, 0.4, and 0.5) g/mL was measured, whereas the estimated osmotic pressure values were listed in Table 3.

These osmotic pressures were much higher than that of seawater (26 atm) [47]. The high osmotic pressure was attributed to the favourable characteristics of K-CQDs and Na-CQDs, namely ultra-small size and rich ionic species. It can be noted from Fig. 4 that the relationship between the osmolality and concentration is linear at the low concentrations measured by the device. Table 3 shows the calculated values of osmolarity and osmotic pressure of the draw solutions at concentrations higher than the measurement range of the device using the obtained linear correlations in Fig. 4. The lower osmotic pressure of Na-CQDS compared to K-CQDs may be attributed to the size of the particles and the characteristics of the material such as solubility and stability. The osmolality of DS depends on their solubility in water and ionization. This result was in good agreement with that reported in [47]. It is worth noting that the osmolality of K-CQDs and Na-CQDs is high which is one of the important advantages that it possesses compared to a lot of materials found in the literature, for example thermos-responsive copolymer PSSS-PNIPAM solution 15SN (33.3 wt%) with osmolality 2137 mosmol/Kg [43], polyelectrolyte [IBMA-Na] solution with osmolality (2600 mosmol/Kg) at concentration of (0.4) g/mL [41] and 0.5 M $MgCl_2$ + 0.05 M $Al_2(SO_4)_3$ with osmolality 2250 mosmol/Kg [47].

3.2. Performance evaluation of FO system

The experiments were carried out for the CTA membrane using K-CQDs, Na-CQDs, and NaCl as draw agents and DI water, synthetic seawater 3.5 wt% NaCl, and pre-filtered Persian Gulf water as feed solutions. The flow rate for both sides is constant at 0.5 L/min. The concentration of K-CQDs and Na-CQDs was 0.3–0.5 g/mL while the NaCl concentration was 80 g/L (0.08 g/mL). The FS was facing the membrane active layer and the DS was facing the membrane support layer. The temperature was kept at 29 ± 1 °C. NaCl was chosen as a reference to benchmark the performance of DS, K-CQDs and Na-CQDs when the feed solution was DI water.

3.2.1. Effect of draw solution concentration and type on permeate flux

The main parameter that can affect the water flux is the driving force (Δπ). The driving force was the difference in osmotic pressures across the membrane between the draw and feed solution sides. Fig. 5 illustrates the water flux for three different feed solutions; DI water, synthetic seawater (3.5 wt% NaCl), and Persian gulf water, respectively. The concentration of the DS was varied between 0.3 and 0.5 g/mL for K-CQDs and Na-CQDs, while fixed at 80 g/mL for the NaCl.

As could be seen in Fig. 5A, a clear gradual increase in water flux was witnessed as the concentration of the DS increased from 0.3 g/mL to 0.5 g/mL for both K-CQDs and Na-CQDs. K-CQDs exhibited 13.924 LMH at

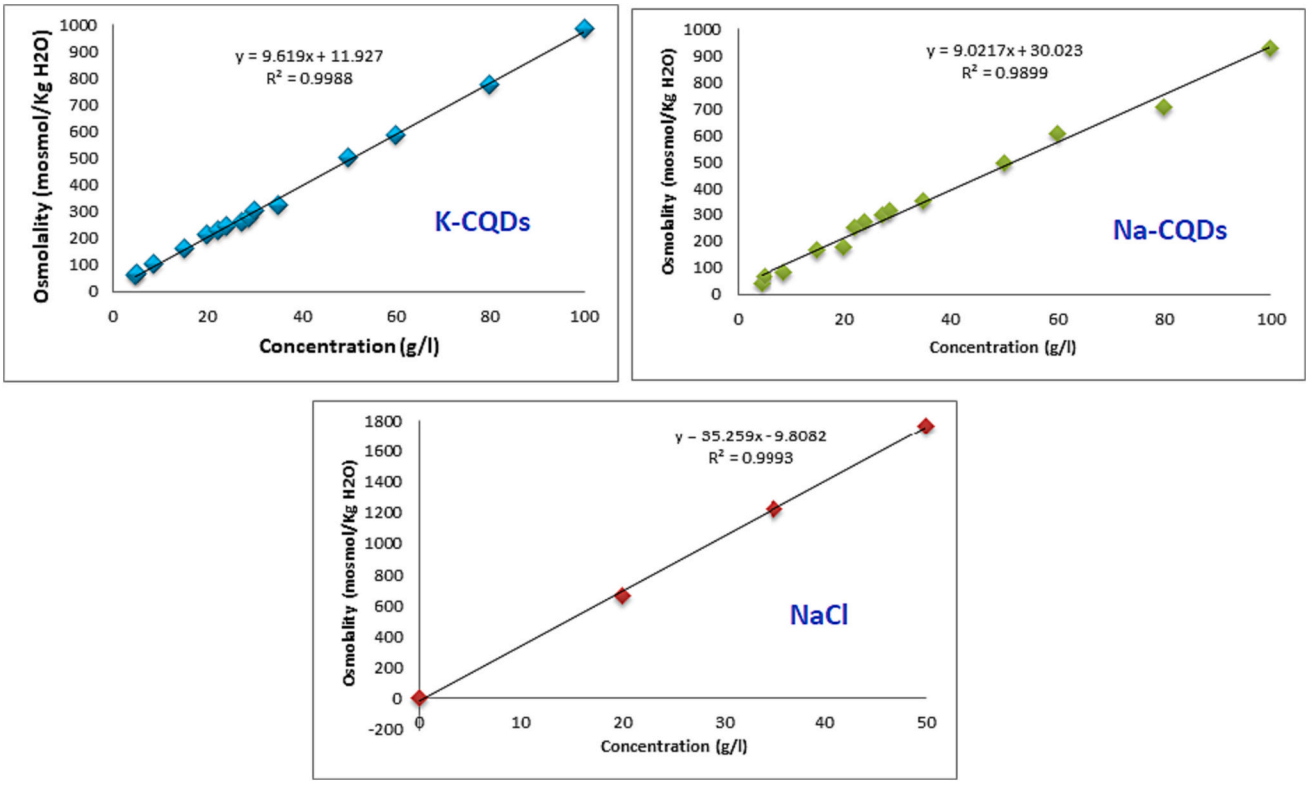

Fig. 4. The relation between osmolality and concentration for (K-CQDs), (Na-CQDs) and NaCl.

Table 3
The predicted osmolality for different draw solutions of different concentrations at a temperature of 29 °C.

Type of DS	Concentration (g/mL)	Osmolality (mosmol/Kg H_2O)	Osmotic pressure (bar)
K-CQDs	0.3	2897.627	72.7437
K-CQDs	0.4	3859.527	96.8918
K-CQDs	0.5	4821.427	121.0399
Na-CQDs	0.3	2736.533	68.6995
Na-CQDs	0.4	3638.703	91.3481
Na-CQDs	0.5	4540.873	113.9967
NaCl	0.035	1224.2568	30.7344
NaCl	0.08	2810.9118	70.5667

0.5 g/mL compared to 10.940 LMH at 0.3 g/mL. However, Na-CQDs showed 11.935 LMH and 10.343 LMH at a concentration of 0.5 and 0.3 g/mL, respectively. Likewise, using NaCl as DS and water as FS, the water flux recorded 14.7 LMH, at the same conditions. When utilizing synthetic seawater as FS, the flux suffered a dramatic decrease for both K-CQDs and Na-CQDs.

Fig. 5B illustrates the permeate water flux of K-CQDs and Na-CQDs as a function of concentration (i.e., 0.3 to 0.5 g/mL) when FS is seawater 3.5 wt% NaCl at 29 °C and the flow rate of FS and DS is 0.5 L/min. As both DS concentrations increased from 0.3 to 0.5 g/mL, the water flux displayed 3.779–5.371 LMH and 1.591–2.785 LMH for K-CQDs and Na-CQDs. The permeate water flux of K-CQDs at a concentration of 0.5 g/mL was larger than that of Na-CQDs at various concentrations (0.3–0.5) g/mL. K-CQDs have a permeate water flux at a concentration of 0.4 g/mL approximately similar to Na-CQDs at a concentration of 0.5 g/mL. The higher flux for K-CQDs as opposed to Na-CQDs is attributed mainly to the higher osmotic pressure and solubility of the former compared to the latter. The structural and surface properties of the draw solutes were main factors influencing the flux values and desalination efficiency of FO process. The average roughness (Ra) (i.e., the arrangement of the physical features of a draw solutes) for K-CQDs was 1.14 nm, while it was 1.3 nm for Na-CQDs. The surface roughness could impact water adsorption onto the CQDs, the lower the roughness, the leaas water retained, and consequently more water available for passage through the membrane. Also, the CTA membrane was in contact with the K-CQDs and Na-CQDs, and the charge of the CTA membrane, K-CQDs and Na-CQDs based on the zeta potential test was positive, which means that the K-CQDs and Na-CQDs were rejected due to electrostatic repulsion. This is beneficial to prevent the deposition of both draw solutes on the surface of the CTA membrane. This finally enhances the water flux and reduces the reverse solute flux that occurs during the FO process.

NaCl has a slightly larger permeate water flux at 80 g/L than K-CQDs and Na-CQDs at 0.5 g/mL. This is due to the low molecular weight, and high osmotic pressure generated but the NaCl solution has the drawback of having a high reverse solute flux and fouling.

Permeate water flux of K-CQDs and Na-CQDs when FS is Persian gulf water at a concentration of 0.5 g/mL at 29 °C and the flow rate of FS and DS is 0.5 L/min as illustrated in Fig. 5C. It can be noticed that using Persian gulf water as FS resulted in 6.16 LMH and 3.779 LMH at 0.5 g/mL for K-CQDs and Na-CQDs, respectively. This observed higher flux at higher DS concentration (0.5 g/mL) was attributed to the increment in the osmotic driving force across the membrane for both DS types. Moreover, the flux manifested an approximately linear increase when the concentration increased from 0.3 to 0.5 g/mL. That could be attributed to the lower viscosity, higher osmotic pressure, molecular weight larger than the pore size of the membrane and the solubility of K-CQDs and Na-CQDs. The results indicate that water flux mainly depends not only on the concentration of the draw solution but also on the type of draw solution. It can be seen from the figures that the water flux for K-CQDs is greater than Na-CQDs. Yet, the water flux of K-CQDs and Na-CQDs was higher than other DS reported in the preceding literature using the same FO membrane [47,49–51].

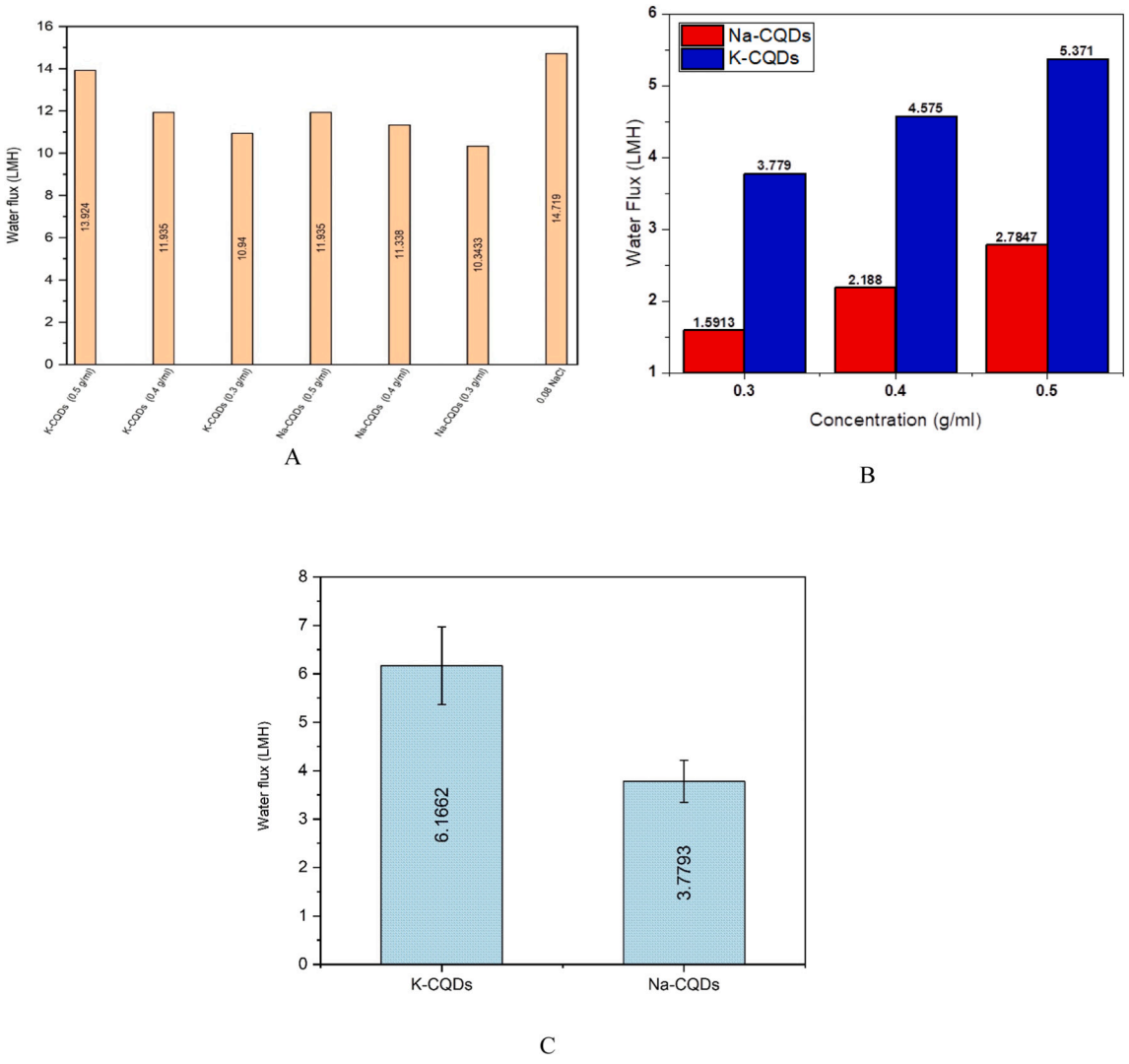

Fig. 5. (A) Permeate water flux of K-CQDs, Na-CQDs and NaCl as a function of concentration for FS of DI water at 29 °C and the flow rate of FS and DS is 0.5 L/min, (B) Permeate water flux of K-CQDs and Na-CQDs as a function of concentration for FS of seawater 3.5 wt% NaCl at 29 °C and the flow rate of FS and DS is 0.5 L/min, (C) Permeate water flux of K-CQDs and Na-CQDs for FS of Persian gulf water and concentration of 0.5 g/mL at 29 °C and the flow rate of FS and DS is 0.5 L/min.

3.2.2. Effect of feed solution concentration on permeate water flux, reverse solute flux (J_s) and specific reverse solute flux (J_s/J_w)

By increasing the salinity of the feed solution from DI water (zero NaCl), seawater (3.5 wt% NaCl) to perian gulf seawater (>3.5 wt% NaCl) respectively, naturally, the driving force decreases according to Eq. (10). This appears as a decrease in water flux through the membrane.

$$\text{Net driving force} = (\pi(\text{draw solution})) - (\pi(\text{feed solution})) \quad (10)$$

Fig. 6 shows the effect of different feed solution concentrations and K-CQDs and Na-CQDs as draw solutions on the FO performance. The water flux of the Persian gulf seawater of K-CQDs and Na-CQDs is (6.1662 LMH) and (3.779 LMH) at 0.5 g/mL, respectively. While the synthetic seawater (3.5 wt% NaCl) is 5.371 LMH and 2.785 LMH at 0.5 g/mL, respectively. It is clear from these figures that at the same concentration of 0.5 g/mL for K-CQDs and Na-CQDs as draw solutions, the water flux of Persian gulf water was higher than the synthetic seawater (3.5 wt% NaCl). The reason for this observation is that the concentration of salt for RPG water is lower than 3.5 wt% NaCl due to this fact that the RPG water has different types of ions as illustrated in EDX test in Fig. S2. This difference in type of ions could lead to a lower osmotic pressure compared to the synthetic seawater, which only has pure NaCl.

The reverse solute flux (RSF) and specific reverse solute flux (SRSF) of K-CQDs and Na-CQDs for various concentrations of 0.3–0.5 g/mL were measured and compared with that of NaCl. A trivial increase in RSF and SRSF associated with the increase in the concentration of K-CQDs and Na-CQDs was noticed accordingly (Fig. 6). This was attributed to the increased osmotic pressure of the DS upon increasing their concentrations. The reverse solute flux of K-CQDS and Na-CQDs when FS was DI water were (0.0161–0.0253) gMH and (0.0414–0.0621) gMH, respectively at different concentrations (0.3–0.5 g/mL). While the RSF of NaCl is 3.9084 gMH at 0.08 g/mL. Also, the specific reverse solute flux (Js/Jw) for K-CQDs and Na-CQDs are (0.0015–0.0018)g/L and (0.0040–0.0052)g/L, respectively at different concentrations (0.3–0.5 g/mL). While the SRSF of NaCl is 0.2655 gMH at 0.08 g/mL. From the figures, one can see that the RSF and SRSF values of K-CQDs and Na-CQDs are negligible compared to NaCl. Because they have very high solubility and the molecular weight of particles is larger than the pore size of the CTA membrane. The RSF and SRSF of K-CQDs are smaller than Na-CQDs due to their very high solubility, low viscosity and high positive charge. Also, the CTA membrane was in contact with the K-CQDs and Na-CQDs, and the charge of the CTA membrane, K-CQDs and Na-CQDs based on the zeta potential test was positive, which means that the K-CQDs and Na-CQDs were rejected due to electrostatic repulsion. This reveals one of the advantages of using K-CQDs and Na-CQDs as a

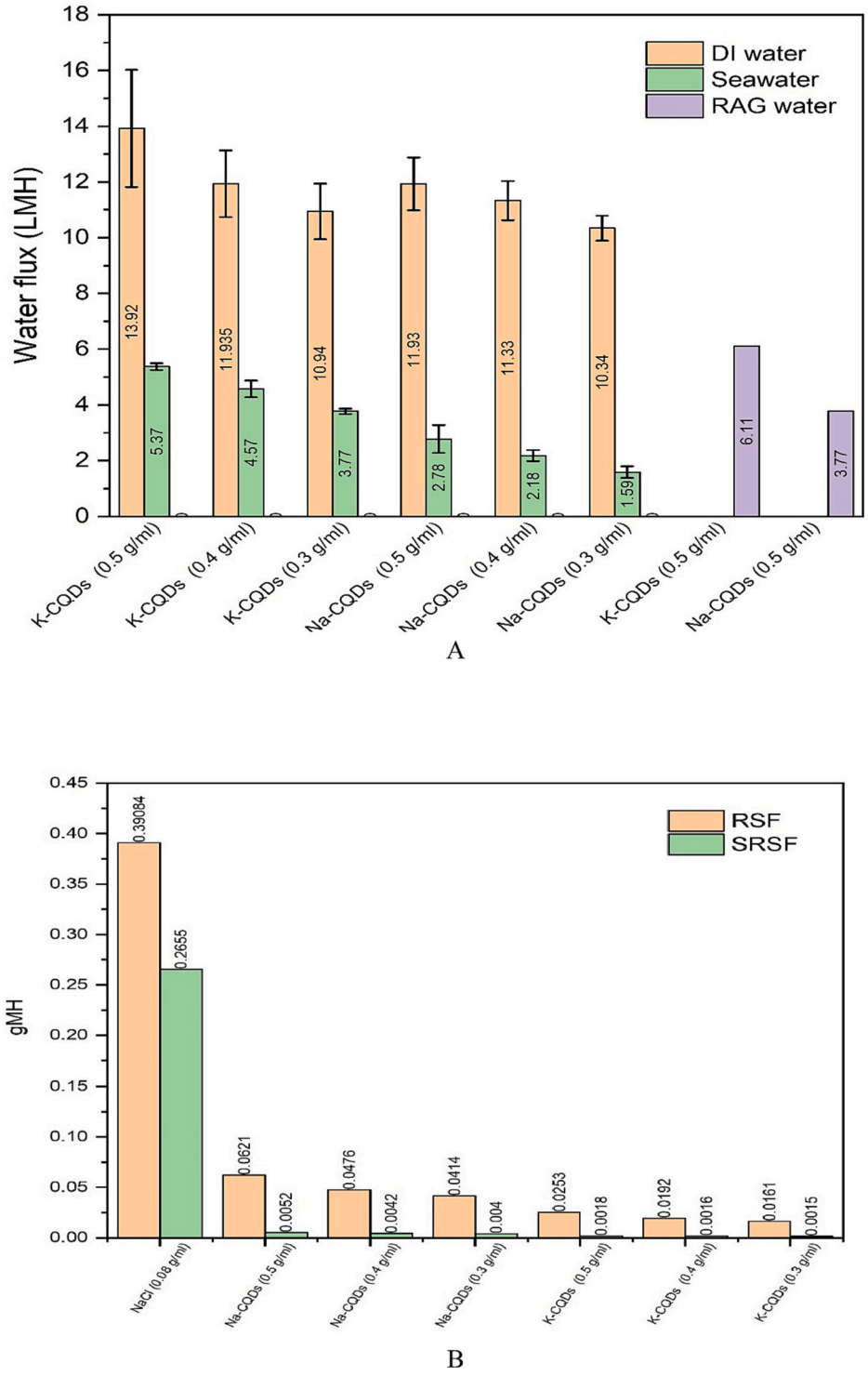

Fig. 6. (A) Permeate water flux as a function of the concentration of feed solution with different concentrations of K-CQDs and Na-CQDs at 29 °C and flow rate FS and DS (0.5 L/min), (B) Reverse solute flux and Specific reverse solute flux of K-CQDs, Na-CQDs as a function of concentration and NaCl (0.08 g/mL) when FS is DI water.

draw solute in the FO process. A novel draw solution for minimizing the reverse flux of ions during FO desalination to decrease the cost of replenishing lost draw solutes. Those findings agreed with a previous work conducted by Guo et al., that has the RSF of Na-CQDs <0.05 gMH [34]. The RSF and SRSF of K-CQDs and Na-CQDs were much lower than other draw solutions mentioned in the preceding literature [47,49,51].

3.2.3. *The recyclability of K-CQDs*

Since K-CQDs should superiority in this study, its recycalbaility was carefully examined. A high thermal decomposition temperature of K-CQDs may enable the stability and recyclability of a draw solute in real applications. In lab-scale testing, the water content of the draw solution (dilute K-CQDs at 0.5 g/mL) when the feed solution is DI water is dried using an oven at 80 °C to recover the K-CQDs powder. The recovered K-CQDs showed a slight or no performance decrease in FO tests compared

to freshly prepared draw solutes when testing for three cycles. Fig. 7 shows the performance of FO water flux at 0.5 g/mL K-CQDs and DI water as feed solution when recycling for using three cycles. The water flux for the respective three cycles was 13.924 LMH, 13.586 LMH, and 13.645 LMH. It is clear from the figure after 3 cycles, the water flux dropped only by 2 % which agrees with the literature [49].

4. Comparison study

This comparison present a deep understanding of how K-CQDs and Na-CQDs as a draw agents performs comparing to other draw agents found in the literature. Table 4 summarized a performance of a number of draw solutes presented in the literature compared to the performance of the K-CQDs and Na-CQDs synthesized in the current study using CTA as a FO membrane. From the comparative results, it can be demonstrates that the K-CQDs and Na-CQDs shows acceptable and comparable FO performance compared with other draw solutes. Additionally, the K-CQDs and Na-CQDs synthesized in this study also manifested an efficient and superior FO performance over those available draw solutes presented in the literature. The K-CQDs and Na-CQDs fabricated by this work has demonstrated promising ability to reach scalability or commercialized if compared with currently available draw solutes.

5. Conclusions

Synthesis and testing K-CQDs and Na-CQDs as promising DS agents were successfully performed and their potential for desalination via FO setup was examined. The following conclusions can be drawn:

1. The TGA analysis proved the sufficient thermal stability of DS which is essential for the FO-MD hybrid process.
2. The water flux increase when the concentration of the draw solution increase for K-CQDs and Na-CQDs in the FO system which is due to the resulting increase in the osmotic pressure while having very low reverse solute flux and specific reverse solute flux compared to other draw solutions reported in the literature.
3. For K-CQDs as a draw solute, the FO water flux is high as 13.924 LMH, RSF and SRSF were negligible with 0.0253 gMH and 0.0018, respectively for a concentration of 0.5 g/mL at 29 °C using DI water as a feed solution. When the feed solution was seawater (3.5 wt% NaCl and Persian Gulf seawater), the water flux of K-CQDs was 5.371 LMH and 6.1662 LMH, respectively. K-CQDs performed better than Na-CQDs with water flux of 11.935 LMH, RSF of 0.0621 gMH, and SRSF of 0.0052 for a concentration of 0.5 g/mL at 29C with DI. When the feed solution was changed to seawater (3.5 wt% NaCl and Persian Gulf water), the water flux of Na-CQDs was 2.7847 LMH and 3.7793 LMH, respectively.
4. The recovered K-CQDs showed a slight or no performance decrease in FO tests compared to freshly prepared draw solutes when testing for three cycles with the loss of flux of only 2 %..
5. Generally our laboratory scale study demonstrated the feasibility of using K-CQDs and Na-CQDs in the FO process and their applicability for seawater desalination.
6. Like any other new draw agents, implementation of CQDs nanoparticles in FO desalination will creates new challenges. From one side, preparation of these nanoparticles requires heating to 180 °C. Providing this temperature on a large scale could have some environmental impacts. On the other hand, separation of these particles from desalinated water and their regeneration by nanofiltration could add extra cost to the process.

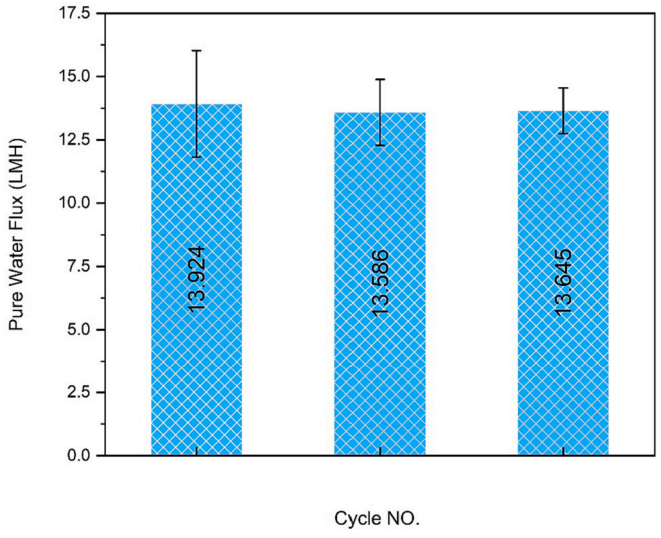

Fig. 7. Performance of permeate water flux at 0.5 g/mL of K-CQDs and DI water as feed solution when recycling for using three cycles.

The promising results obtained in this study should motivate further future work to test these draw solutions with the other FO orientation (e.g. pressure retarded osmosis). Longer tests for filtration and recyclability would also be useful to explore in the future. While the impact of temperature on the prepared CQDs structure was explored through TGA analysis, a further examining of the temperature effect on CQDs performance in water would be beneficial to assess their feasibility in FO-MD systems.

Funding

The authors acknowledge funding by the German Federal Ministry of Education and Research within the MEWAC program under project No. 02WME1613.

CRediT authorship contribution statement

Afraa H. Kamel: validation, formal analysis, investigation, data curation, and writing - original draft preparation.

Qusay F. Alsalhy: conceptualization, methodology, validation, formal analysis, investigation, data curation, writing - original draft preparation, writing - review and editing, visualization, supervision.

Salah S. Ibrahim: conceptualization, methodology, validation, formal analysis, investigation, data curation, supervision.

Khalefa A. Faneer: validation, formal analysis, and investigation.

S. Abdollatif Hashemifard: validation, formal analysis, investigation, writing - review and editing, visualization.

A. Jangizehi: validation, formal analysis, investigation, writing - review and editing, visualization.

S. Seiffert: validation, formal analysis, investigation, writing - review and editing, visualization.

Michael Maskos: validation, formal analysis, investigation, writing - review and editing, visualization.

Alireza Shakeri: validation, formal analysis, investigation, writing - review and editing, visualization.

Christoph bantz: formal analysis, and investigation.

Declaration of competing interest

The authors declare that they have no known competing financial interests or personal relationships that could have appeared to influence the work reported in this paper.

Data availability

No data was used for the research described in the article.

Table 4
Performance comparison of K-CQDs with different draw solutes found in the literature.

Membrane material	Feed	Draw solute	Concentration	Osmotic Pressure	FO Performance		Ref.
					Jw (LMH)	(Js) gMH	
CTA	Ultrapure water	$KHCO_3$	1.4 (M)	2.8 MPa	5.54	1.2	[11]
CTA	Ultrapure water	KBr	0.6 (M)	2.8 MPa	10.22	22	[11]
CTA	Ultrapure water	KCl	47 (g/L)	2.8 MPa	10.9	12.3	[11]
CTA	Ultrapure water	MgSO4	141.3 (g/L)	2.8 MPa	5.5	1.2	[11]
CTA–polyester screen	Distilled water	NaCl	0.6 (M)	27.44 bar	6.3	7.25	[52]
CA	DI water	Fe complex; (Fe-CA)	1 (M)	–	10.78	0.12	[53]
					21	0.14	
CTA	DI water	Poly(isobutylene-alt-maleic acid) sodium salt	0.375 (g/mL)	–	34	0.196	[47]
CTA	DI water	Thermo-responsive PNIPAM/γ-PGA/PEG	0.20 (g/L)	–	1.99	–	[54]
	NaCl 0.05 %	hydrogel			1.7		
	0.1 %				1.3		
	0.2 %				1.1		
CTA	Seawater	fertilizer (multicomponent)	22 (g/L)	–	4.3	0.80	[55]
CTA	DI water	NaCl	1.17×10^2 (g/L)	–	14.47–18.82		[56]
CTA	Seawater	K-CQDs	0.5 (g/L)	121.0399 bar	5.371	0.39084	This work
CTA	Persian Gulf	K-CQDs	0.5 (g/L)	121.0399 bar	6.1662	0.0253	This work
CTA	DI water	K-CQDs	0.5 (g/L)	121.0399 bar	13.924	–	This work

Appendix A. Supplementary data

Supplementary data to this article can be found online at https://doi.org/10.1016/j.desal.2023.116956.

References

[1] D. Johnson, N. Hilal, A.F. Ismail, M. Khayet, Osmosis Engineering, 2021.
[2] D. Johnson, R. Hashaikeh, N. Hilal, Basic principles of osmosis and osmotic pressure, in: Osmosis Engineering, Elsevier, 2021, pp. 1–15.
[3] M. Al-Shaeli, R.A. Al-Juboori, S. Al Aani, B.P. Ladewig, N. Hilal, Natural and recycled materials for sustainable membrane modification: recent trends and prospects, Sci. Total Environ. 838 (2022) 156014.
[4] R.A. Al-Juboori, M. Al-Shaeli, S.A. Aani, D. Johnson, N. Hilal, Membrane technologies for nitrogen recovery from waste streams: scientometrics and technical analysis, Membranes 13 (1) (2022) 15.
[5] N.Z.S. Yahaya, M.Z.M. Pauzi, N.M.a. Mahpoz, M.A. Rahman, K.H. Abas, A. F. Ismail, M.H.D. Othman, J. Jaafar, Forward osmosis for desalination application, in: Membrane Separation Principles and Applications, Elsevier, 2019, pp. 315–337.
[6] A. Razmjou, G.P. Simon, H. Wang, Effect of particle size on the performance of forward osmosis desalination by stimuli-responsive polymer hydrogels as a draw agent, Chem. Eng. J. 215 (2013) 913–920.
[7] M. Amjad, J. Gardy, A. Hassanpour, D. Wen, Novel draw solution for forward osmosis based solar desalination, Appl. Energy 230 (2018) 220–231.
[8] G. Gwak, S. Hong, Draw solute selection, in: Membrane-based Salinity Gradient Processes for Water Treatment and Power Generation, Elsevier, 2018, pp. 87–122.
[9] J. Wang, N. Pathak, L. Chekli, S. Phuntsho, Y. Kim, D. Li, H.K. Shon, Performance of a novel fertilizer-drawn forward osmosis aerobic membrane bioreactor (FDFO-MBR): mitigating salinity build-up by integrating microfiltration, Water 9 (1) (2017) 21.
[10] C. Tan, H. Ng, A novel hybrid forward osmosis-nanofiltration (FO-NF) process for seawater desalination: draw solution selection and system configuration, Desalin. Water Treat. 13 (1–3) (2010) 356–361.
[11] A. Achilli, T.Y. Cath, A.E. Childress, Selection of inorganic-based draw solutions for forward osmosis applications, J. Membr. Sci. 364 (1–2) (2010) 233–241.
[12] R.L. McGinnis, J.R. McCutcheon, M. Elimelech, A novel ammonia–carbon dioxide osmotic heat engine for power generation, J. Membr. Sci. 305 (1–2) (2007) 13–19.
[13] C. Boo, Y.F. Khalil, M. Elimelech, Performance evaluation of trimethylamine–carbon dioxide thermolytic draw solution for engineered osmosis, J. Membr. Sci. 473 (2015) 302–309.
[14] R.L. McGinnis, Osmotic desalinization process, Google Patents, 2002.
[15] Z. Li, R.V. Linares, S. Bucs, C. Aubry, N. Ghaffour, J.S. Vrouwenvelder, G. Amy, Calcium carbonate scaling in seawater desalination by ammonia–carbon dioxide forward osmosis: mechanism and implications, J. Membr. Sci. 481 (2015) 36–43.
[16] M.R. Moßhammer, F.C. Stintzing, R. Carle, Evaluation of different methods for the production of juice concentrates and fruit powders from cactus pear, Innovative Food Sci. Emerg. Technol. 7 (4) (2006) 275–287.
[17] J. Kessler, C. Moody, Drinking water from sea water by forward osmosis, Desalination 18 (3) (1976) 297–306.
[18] J.R. Herron, E.G. Beaudry, C.E. Jochums, L.E. Medina, Osmotic concentration apparatus and method for direct osmotic concentration of fruit juices, Google Patents, 1994.
[19] G. Gwak, B. Jung, S. Han, S. Hong, Evaluation of poly (aspartic acid sodium salt) as a draw solute for forward osmosis, Water Res. 80 (2015) 294–305.
[20] Z. Xu, K. Wu, H. Luo, Q. Wang, T.C. Zhang, X. Chen, H. Rong, Q. Fang, Electro-responsive semi-IPN hydrogel with enhanced responsive property for forward osmosis desalination, J. Appl. Polym. Sci. 139 (7) (2022) 51650.
[21] H.T. Nguyen, N.C. Nguyen, S.-S. Chen, H.C. Duong, M.L. Nguyen, C.-S. Tran, P.-D. Nguyen, Exploration of a cost-effective draw solution based on mixing surfactant and sodium chloride for forward osmosis desalination process, Environ. Technol. Innov. 30 (2023), 103088.
[22] A.P. Bendoy, H.G. Zeweldi, M.J. Park, H.K. Shon, H. Kim, W.-J. Chung, G. M. Nisola, Thermo-responsive hydrogel with deep eutectic mixture co-monomer as drawing agent for forward osmosis, Desalination 542 (2022), 116067.
[23] D. Ma, Y. Tian, T. He, X. Zhu, Preparation of novel magnetic nanoparticles as draw solutes in forward osmosis desalination, Chin. J. Chem. Eng. 46 (2022) 223–230.
[24] Z. Pan, Y. Huang, X. Yang, Y. Liang, J. He, H. Yu, Synthesis and characterization of sewage sludge ash-based temperature-sensitive hydrogel as an advanced class of forward osmosis desalination draw agent, Environ. Eng. Sci. 39 (11) (2022) 896–905.
[25] D. Li, X. Zhang, J. Yao, Y. Zeng, G.P. Simon, H. Wang, Composite polymer hydrogels as draw agents in forward osmosis and solar dewatering, Soft Matter 7 (21) (2011) 10048–10056.
[26] D. Li, X. Zhang, J. Yao, G.P. Simon, H. Wang, Stimuli-responsive polymer hydrogels as a new class of draw agent for forward osmosis desalination, Chem. Commun. 47 (6) (2011) 1710–1712.
[27] B. Warne, R. Buscall, E. Mayes, T. Oriard, I. Norris, Water purification method, GB patent 2464956 (2008).
[28] Y. Na, S. Yang, S. Lee, Evaluation of citrate-coated magnetic nanoparticles as draw solute for forward osmosis, Desalination 347 (2014) 34–42.
[29] H. Bai, Z. Liu, D.D. Sun, Highly water soluble and recovered dextran coated Fe_3O_4 magnetic nanoparticles for brackish water desalination, Sep. Purif. Technol. 81 (3) (2011) 392–399.
[30] M. MingáLing, Facile synthesis of thermosensitive magnetic nanoparticles as "smart" draw solutes in forward osmosis, Chem. Commun. 47 (38) (2011) 10788–10790.
[31] X. Zhang, M. Jiang, N. Niu, Z. Chen, S. Li, S. Liu, J. Li, Natural-product-derived carbon dots: from natural products to functional materials, ChemSusChem 11 (1) (2018) 11–24.
[32] L. Zhou, Y. Lin, Z. Huang, J. Ren, X. Qu, Carbon nanodots as fluorescence probes for rapid, sensitive, and label-free detection of Hg^{2+} and biothiols in complex matrices, Chem. Commun. 48 (8) (2012) 1147–1149.
[33] C. Fowley, N. Nomikou, A.P. McHale, B. McCaughan, J.F. Callan, Extending the tissue penetration capability of conventional photosensitisers: a carbon quantum dot–protoporphyrin IX conjugate for use in two-photon excited photodynamic therapy, Chem. Commun. 49 (79) (2013) 8934–8936.
[34] C. XianáGuo, Na+-functionalized carbon quantum dots: a new draw solute in forward osmosis for seawater desalination, Chem. Commun. 50 (55) (2014) 7318–7321.
[35] K. Doshi, A.A. Mungray, Bio-route synthesis of carbon quantum dots from tulsi leaves and its application as a draw solution in forward osmosis, J. Environ. Chem. Eng. 8 (5) (2020), 104174.
[36] D.L. Zhao, T.-S. Chung, Applications of carbon quantum dots (CQDs) in membrane technologies: a review, Water Res. 147 (2018) 43–49, https://doi.org/10.1016/j.watres.2018.09.040.
[37] M. Yasukawa, D. Shigefuji, M. Shibuya, Y. Ikebe, R. Horie, M. Higa, Effect of DS concentration on the PRO performance using a 5-inch scale cellulose triacetate-based hollow fiber membrane module, Membranes 8 (2) (2018) 22.
[38] S.S. Ray, S.-S. Chen, D. Sangeetha, H.-M. Chang, C.N.D. Thanh, Q.H. Le, H.-M. Ku, Developments in forward osmosis and membrane distillation for desalination of waters, Environ. Chem. Lett. 16 (2018) 1247–1265.
[39] Y. Dong, C. Chen, X. Zheng, L. Gao, Z. Cui, H. Yang, C. Guo, Y. Chi, C.M. Li, One-step and high yield simultaneous preparation of single-and multi-layer graphene quantum dots from CX-72 carbon black, J. Mater. Chem. 22 (18) (2012) 8764–8766.

[40] W. Gai, D.L. Zhao, T.-S. Chung, Novel thin film composite hollow fiber membranes incorporated with carbon quantum dots for osmotic power generation, J. Membr. Sci. 551 (2018) 94–102.
[41] Y.-P. Sun, B. Zhou, Y. Lin, W. Wang, K.S. Fernando, P. Pathak, M.J. Meziani, B. A. Harruff, X. Wang, H. Wang, Quantum-sized carbon dots for bright and colorful photoluminescence, J. Am. Chem. Soc. 128 (24) (2006) 7756–7757.
[42] R. Ludmerczki, S. Mura, C.M. Carbonaro, I.M. Mandity, M. Carraro, N. Senes, S. Garroni, G. Granozzi, L. Calvillo, S. Marras, Carbon dots from citric acid and its intermediates formed by thermal decomposition, Chem Eur J 25 (51) (2019) 11963–11974.
[43] T.E. Thomas, S. Al Aani, D.L. Oatley-Radcliffe, P.M. Williams, N. Hilal, Laser Doppler Electrophoresis and electro-osmotic flow mapping: a novel methodology for the determination of membrane surface zeta potential, J. Membr. Sci. 523 (2017) 524–532.
[44] M. Walters, S. Al Aani, P.P. Esteban, P.M. Williams, D.L. Oatley-Radcliffe, Laser Doppler electrophoresis and electro-osmotic flow mapping for the zeta potential measurement of positively charged membrane surfaces, Chem. Eng. Res. Des. 159 (2020) 468–476.
[45] V. Rimal, S. Shishodia, P. Srivastava, Novel synthesis of high-thermal stability carbon dots and nanocomposites from oleic acid as an organic substrate, Appl. Nanosci. 10 (2020) 455–464.
[46] P. Wang, Y. Cui, Q. Ge, T.F. Tew, T.-S. Chung, Evaluation of hydroacid complex in the forward osmosis–membrane distillation (FO–MD) system for desalination, J. Membr. Sci. 494 (2015) 1–7.
[47] R. Kumar, S. Al-Haddad, M. Al-Rughaib, M. Salman, Evaluation of hydrolyzed poly (isobutylene-alt-maleic anhydride) as a polyelectrolyte draw solution for forward osmosis desalination, Desalination 394 (2016) 148–154.
[48] P. Wang, T.-S. Chung, Recent advances in membrane distillation processes: membrane development, configuration design and application exploring, J. Membr. Sci. 474 (2015) 39–56.
[49] S.K. Yen, M. Su, K.Y. Wang, T.-S. Chung, Study of draw solutes using 2-methylimidazole-based compounds in forward osmosis, J. Membr. Sci. 364 (1–2) (2010) 242–252.
[50] N.C. Nguyen, S.-S. Chen, S.-T. Ho, H.T. Nguyen, S.S. Ray, N.T. Nguyen, H.-T. Hsu, N.C. Le, T.T. Tran, Optimising the recovery of EDTA-2Na draw solution in forward osmosis through direct contact membrane distillation, Sep. Purif. Technol. 198 (2018) 108–112.
[51] N.C. Nguyen, H.C. Duong, H.T. Nguyen, S.-S. Chen, H.Q. Le, H.H. Ngo, W. Guo, C. C. Duong, N.C. Le, X.T. Bui, Forward osmosis–membrane distillation hybrid system for desalination using mixed trivalent draw solution, J. Membr. Sci. 603 (2020), 118029.
[52] M. Nematzadeh, A. Samimi, S. Shokrollahzadeh, Application of sodium bicarbonate as draw solution in forward osmosis desalination: influence of temperature and linear flow velocity, Desalin. Water Treat. 57 (44) (2016) 20784–20791.
[53] Q. Ge, T.-S. Chung, Hydroacid complexes: a new class of draw solutes to promote forward osmosis (FO) processes, Chem. Commun. 49 (76) (2013) 8471–8473.
[54] K. Zhang, F. Li, Y. Wu, L. Feng, L. Zhang, Construction of ionic thermo-responsive PNIPAM/γ-PGA/PEG hydrogel as a draw agent for enhanced forward-osmosis desalination, Desalination 495 (2020), 114667.
[55] M. Gulied, F. Al Momani, M. Khraisheh, R. Bhosale, A. AlNouss, Influence of draw solution type and properties on the performance of forward osmosis process: energy consumption and sustainable water reuse, Chemosphere 233 (2019) 234–244.
[56] P. Zhao, B. Gao, Q. Yue, S. Liu, H.K. Shon, Effect of high salinity on the performance of forward osmosis: water flux, membrane scaling and removal efficiency, Desalination 378 (2016) 67–73.